






Received XX Month, XXXX; revised XX Month, XXXX; accepted XX Month, XXXX; Date of publication XX Month, XXXX; date of current version XX Month, XXXX.

Digital Object Identifier 10.1109/OJCOMS.2022.1234567

IMT to Satellite Stochastic Interference Modeling and Coexistence Analysis of Upper 6 GHz Band Service

Reza Aghazadeh Ayoubi¹  (Student Member, IEEE), Dario Tagliaferri¹  (Member, IEEE), Filippo Morandi¹  (Student Member, IEEE), Luca Rinaldi¹ (Student Member, IEEE), Laura Resteghini² (Member, IEEE), Christian Mazzucco²  (Member, IEEE) and Umberto Spagnolini¹  (Senior Member, IEEE)

¹Department of Electronics, Information and Bioengineering (DEIB) of Politecnico di Milano, 20133 Milan

²Huawei Technologies Italia S.r.l., Segrate, 20054 Italy

CORRESPONDING AUTHOR: Reza Aghazadeh Ayoubi (e-mail: reza.aghazadeh@polimi.it).

U. Spagnolini is Huawei Industry Chair at Politecnico di Milano

ABSTRACT The surging capacity demands of 5G networks and the limited coverage distance of high frequencies like millimeter-wave (mmW) and sub-terahertz (THz) bands have led to consider the upper 6 GHz (U6G) spectrum for radio access. However, due to the presence of the existing satellite (SAT) services in these bands, it is crucial to evaluate the impact of the interference of terrestrial U6G stations to SAT systems. A comprehensive study on the aggregated U6G-to-SAT interference is still missing in the literature. In this paper, we propose a stochastic model of interference (SMI) to evaluate the U6G-to-SAT interference, including the statistical characterization of array gain and clutter-loss and considering different interference modes. Furthermore, we propose an approximate geometrical-based stochastic model of interference (GSMI) as an alternative method to SMI when the clutter-loss distribution is unavailable. Our results indicate that given the typical international mobile telecommunication (IMT) parameters, the aggregated interference power toward the geostationary (GEO) SATs, is well below the relevant protection criterion, and we prove numerically that the GSMI method overestimates the aggregated interference power with only 2 dB compared to the SMI method.

INDEX TERMS satellite communication, U6G, 6G, aggregated interference, stochastic geometry

I. INTRODUCTION

THE coexistence of satellite (SAT) communications with fifth-generation (5G) and beyond 5G (B5G) base station (BS) operating in the upper 6GHz (U6G) frequency is an arising issue due to the growing interest in new bands to increase capacity in densely populated areas [1]–[4]. Studies demonstrate that the usage of the upper mid-band is necessary to fulfill the requirements of the downlink of 5G [5]. At the same time, around 40% of the benefit foreseen for 5G mid-bands will not be exploited in the absence of a new mid-bands spectrum assignment [6]. These additional frequencies provide large bandwidth, in excess of 100 MHz, while characterized by a smaller path loss compared to

millimeter-wave (mmW) 5G [7]. The deployment of new U6G systems might affect the operation of SATs already in place that use these frequency bands in uplink [7], such as C-band (4-8 GHz) and X-band (8-12 GHz) [8]. Even if the emission of a single BS serving all user equipment (UE) has a negligible impact on SAT, the aggregation of the interference from a large number of BSs in a large area (e.g., the satellite footprint (SATFP) on Earth) might be comparable with the interference sensitivity threshold, and thus the coexistence of SAT communications with IMT communications must be managed [9]. In [10], the effect of the interference on geosynchronous synthetic aperture radars has been studied in the context of remote sensing in the C-

band. However, the sources of interference are different w.r.t the international mobile telecommunications (IMT).

Currently, there are no comprehensive studies regarding the statistical analysis of aggregated interference from BSs, observed by the SATs in the U6G bands. The coexistence analysis between IMT-2020 and SAT systems has been widely studied (see, e.g., [11]–[17]) mostly for mmW bands (24.25 and 86 GHz), and in the context of relevant agendas (see e.g., [18] or international telecommunications union (ITU) agenda WRC-23 item 1.2). The previous works usually target the aggregated interference in the SATFP considering only the direct BS-SAT path. Moreover, they all consider the same propagation model, valid for frequencies above 10 GHz (see [19] for further details). Therefore, it is clear that existing interference modeling approaches cannot be readily extended to the U6G spectrum, since (i) the propagation model is not appropriate for frequencies < 10 GHz, and (ii) different interference modes are typically neglected. The term interference mode is herein used for any propagation that ends up toward the SAT, including the direct BS-SAT path or reflections (from the ground or buildings towards the SAT).

The problem of interference estimation in communication systems involves the modeling of both the U6G devices (deployment, functioning, antennas, etc.) and propagation for the involved frequencies and environments. Several guidelines to evaluate the compatibility between terrestrial and space stations are provided in the literature. The work in [20] presents a methodology for modeling IMT-Advanced, namely fourth-generation (4G), and IMT-2020 (5G), networks, and systems for general coexistence studies. It details the simulation setup, including the modeling of network topology and antenna arrays. The methodology is based on the characteristics of IMT-advanced systems [21].

Besides system modeling, it is necessary to determine a suitable propagation model for earth-space interference evaluation [22], including all the relevant phenomena such as clutter loss, which is an additional loss with respect to the path-loss, created by the diffraction, reflection, or scattering of the buildings and vegetation in the vicinity of the BSs.

An empirical model for the cumulative distribution function (CDF) of the clutter loss is reported in [19], for earth-space links working above 10 GHz. This latter model can be used when the geometry of the scenario is not known. In contrast, when prior information on the environment is available, e.g., statistical characterization of the geometrical features, the stochastic model in [23] might be applied, provided that appropriate modifications are made to extend its validity below 10 GHz. Utilizing a stochastic model circumvents the need for computationally expensive ray tracing-based methods, while site-specific modifications to the results are easily made by adjusting the statistical distributions of the parameters in each geographical region.

The main contribution of this paper is the development of a stochastic method that can be used to evaluate the

aggregate interference at a geostationary (GEO) SAT from U6G terrestrial BSs. The proposed method is general since it does not constrain the analysis to any specific scenario, but can extend to others upon proper adaptation of earth-space propagation and antenna array modeling.

The detailed contributions are listed in the following:

- We develop an stochastic model of the interference (SMI) towards a SAT from a set of micro and macro BSs, based on a stochastic description of the BS array gain and clutter loss, calculated according to the geometrical distribution of a given region. We use a characteristic function (CF)-based approach, to efficiently aggregate all the interference power, from different types of BSs, when serving both indoor and outdoor UEs, to ultimately yield a methodology for estimating the aggregated interference power from the SATFP.
- We propose a geometry-based stochastic model of the interference (GSMI) method to estimate the aggregated interference at the SAT when no clutter-loss statistics are available. The GMSI method leverages the environment's geometrical statistics.
- We provide numerical examples of the interference CDF for U6G service with the SMI and GSMI methods. Our results demonstrate that, given typical parameter values, the aggregated interference power from U6G is well below the interference to noise ratio (INR) protection criterion, while it is relevant only for extreme values of the employed parameters. We show that the GSMI results overestimate the interference power density by only 2 dB with respect to SMI results, on aggregate for the SATFP.

Organization: The remainder of the paper is organized as follows: in Sec. II we present the system model. In Sec. III and Sec. IV, the methodology for modeling the interference from a single BS and from BSs in a large region are presented, respectively. The distribution of the array gain and clutter-loss are discussed in Sec. V and Sec. VI. In Sec. VII, the process of extracting the geometrical statistics is discussed. The numerical results are in Sec. VIII and the paper is concluded in Sec. IX.

II. System Model

Modeling the aggregated interference to a SAT from a set of BSs requires both geometrical and propagation considerations. Let us consider the scenario in Fig. 1, where a single BS at height h_{BS} is causing interference to the SAT while serving a single-antenna ground UE. The coordinate system is such that an arbitrary set of angles $\vartheta = (\psi, \phi)$, consists of azimuth angle $-180 < \phi \leq 180$ deg, defined as clockwise positive from North, and elevation angle defined as $-90 < \psi \leq 90$ deg relative to the ground plane, located at the BS height. The SAT, given a longitude and latitude of observation, is identified by the angle of departure

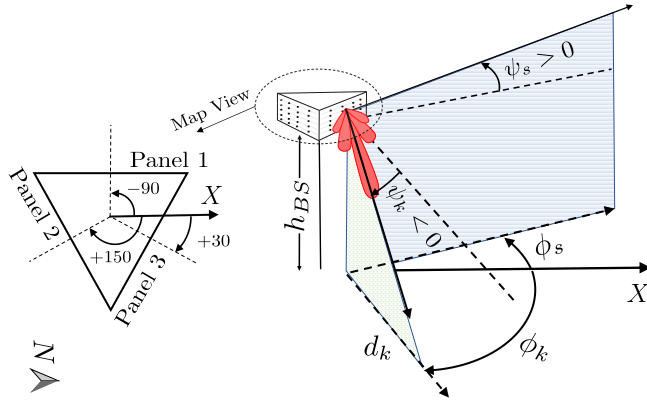


FIGURE 1: Tri-sectoral BS serving a UE, while unwillingly generating at the SAT.

(AoD) $\vartheta_s = (\psi_s, \phi_s)$ from the BS. In this setting, $\psi < 0$ correspond to any interference mode that first bounces on the ground. The same coordinate system is used for the served UE at $\vartheta_k = (\psi_k, \phi_k)$. A set of stochastic parameters Θ characterizes the environment, UE, and the BS distributions, including: (i) inter-building distance d ; (ii) BS-building distance; (iii) the BS height h_{BS} ; (iv) buildings height h ; (v) UEs height h_{UE} . The signal received by the k -th UE from a single BS is

$$y_k = \sqrt{P_T G_a(\vartheta_k|\vartheta_k, \Theta)} \alpha_k x_k + w_k, \quad (1)$$

where x_k is the Tx signal, $G_a(\vartheta_k|\vartheta_k, \Theta)$ is the array gain toward the UE of interest, when the BS array is designed to points toward ϑ_k (Fig. 2), P_T is the Tx power and α_k the path-loss for distance d_k , including any shadowing and fading and w_k is the noise amplitude. For a given position and height of the BS, the signal (1) toward the UE, generates interference at SAT. This is originated from either the direct path (i.e. at angle ϑ_s), and/or from other interference modes. For example, the signal x_k might be reflected by ground/buildings toward the SAT, or it might be diffracted by vegetation/building edges. Let ϑ_ℓ denote the AoD of the rays in ℓ -th propagation mode, which is a function of ϑ_s (e.g., for direct BS-SAT propagation mode, it is $\vartheta_\ell = \vartheta_s$). The interfering signal received by the SAT, when the q -th BS is serving the k -th UE (ℓ -th interference mode) is

$$i_{q,k}^\ell(\Theta) = \sqrt{G_a(\vartheta_\ell|\vartheta_k, \Theta) \frac{P_T}{A_c(\vartheta_\ell|\Theta)}} \alpha_s x_k + w_s, \quad (2)$$

where $G_a(\vartheta_\ell|\vartheta_k, \Theta)$ is the BS array gain toward ϑ_ℓ when it is designed to points to ϑ_k , $A_c(\vartheta_\ell|\Theta)$ is the clutter loss between the BS and SAT, w_s is the additive white Gaussian noise with power spectral density (PSD) N_0 over bandwidth B , while α_s consists of all the phenomena above the terrain as

$$\alpha_s = \frac{G_s}{A_s A_{pol}}, \quad (3)$$

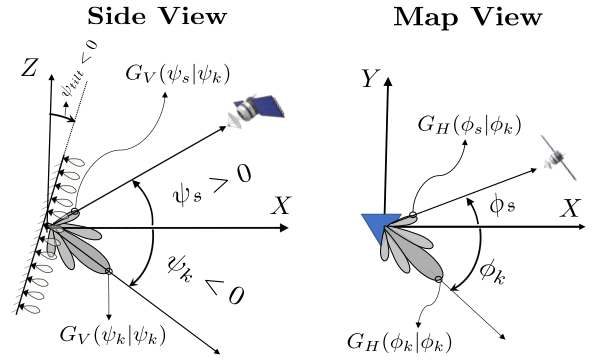


FIGURE 2: Map view and side view of the tri-sectoral panels.

where G_s , A_s , and A_{pol} are respectively the SAT antenna gain, the free space path loss, and the loss due to polarization mismatch. The dependence of the array gain and clutter loss on the set of geometrical parameters Θ , and the interference modes is detailed in Sec. V and Sec. VI. Note that the beam spread loss, which is the loss caused by refractive effects of the atmosphere, is neglected since it is only relevant for very small elevation angles [24], and atmospheric gases absorption is typically neglected around 6 GHz [8], [25].

Although the largest part of the aggregated interference comes from the direct BS-SAT path, all the other interference modes cannot be neglected, otherwise, the interference is underestimated. The aggregated interference power caused by Q total BSs each serving K possible UEs, through L possible interference modes, is

$$I(\Theta) = \sum_{q=1}^Q \sum_{k=1}^K \sum_{\ell=1}^L I_{q,k}^\ell(\Theta), \quad (4)$$

where $I_{q,k}^\ell(\Theta) = (i_{q,k}^\ell(\Theta))^2$ is the single interference power contribution. In practice, the number of served UEs K is not deterministic, and the aggregation over all the served UEs can be replaced by modeling the transmit power P_T with an appropriate probability density function (PDF) or the BS loading factor. Thus, herein the UE index k in (4) will be dropped with the corresponding summation. Note that the loading factor is a parameter recommended by standardization bodies [26], [27], which is used to represent the average transmit power of the BSs for the ensemble of UEs.

BSs can be modeled as transmitting with full power (On) or not transmitting at all (Off) [20], with a loading factor ρ defined as the percentage of the BSs that are randomly chosen as active. Furthermore, each BS transmit only a fraction of total time F_T , due to employing time division duplex (TDD). Each BS is either a macro BS or a micro BS, as shown in Fig. 3. Macro BSs employ larger array sizes, organized in three sectors to cover multiple cells, a higher transmitter power P_T , and a larger height compared to micro BS. We assume, without any loss of generality,

that macro BSs are placed on top of the tallest building in each area [20], for coverage purposes. Differently, micro BSs have a single sector, and they are characterized by a reduced Tx power and are mostly aimed at boosting coverage and capacity at cell edges. Thus, for mere modeling purposes, we assume the micro BS is located on the ground, at the furthest distance from the macro one. Considering a single BS, its height from ground h_{BS} as well as its position with respect to surrounding buildings can be regarded as random. This affects the modeling of the interference modes toward the SAT, which can be evaluated in a probabilistic framework, using the geometrical statistics of the environment.

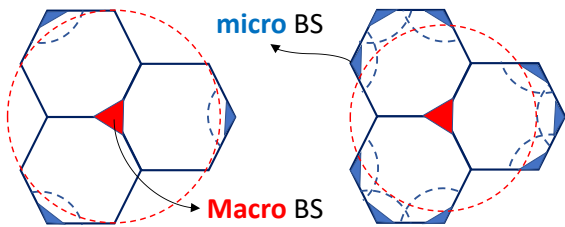


FIGURE 3: Macro and micro BS arrangement. Every cell is covered with one or multiple micro BSs. Each micro BS has a single sector array, that serves the edge UEs of the corresponding macro cell.

III. Statistical Model of Interference from a Single BS

The aggregated interference experienced by SATs is evaluated herein through stochastic models since the involved phenomena are inherently stochastic, capturing the complex and dynamic behavior of each phenomenon. This section presents the statistical framework to evaluate the interference at the SAT, using both SMI and GSMI methods, provided that the statistical distributions of the involved phenomena (e.g. array gain and clutter loss) are known or properly inferred. Then, Sections V and VI detail how the aforementioned statistical distributions are acquired.

In the SMI method, all the possible interference modes (from every possible bounce of the rays) are considered to occur, and each propagation path is subject to a specific clutter loss, with a corresponding probability distribution. In the GSMI method instead, the interference modes are limited to the significant ones, each of these occurring with a specific probability, while the clutter loss is not considered. A main difference between the two methods is that the PDF of the clutter loss in the SMI method is achieved by ray tracing. Instead, the GSMI makes use of stochastic geometry to approximate clutter loss.

A. Stochastic model of interference (SMI)

In the SMI method, the interference is evaluated by considering every possible interference mode that reaches the SAT with any number of bounces. The SMI method requires knowledge of the PDF of both array gain and clutter-loss

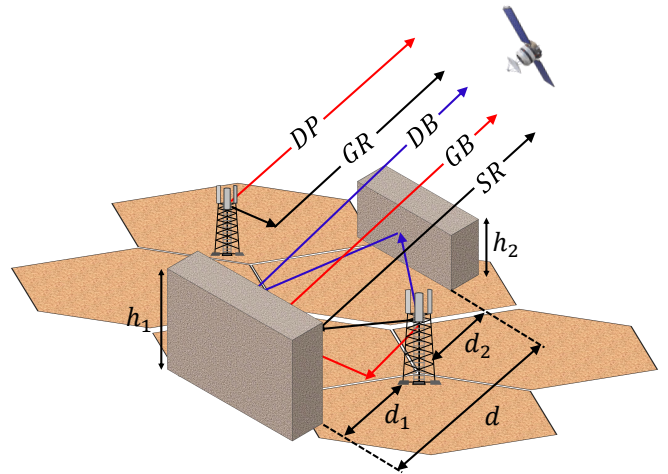


FIGURE 4: Interference modes of GSMI method for two micro BSs including the Direct path (DP), single-building (SB) reflection, double building (DB) reflection, ground reflection (GR), ground and building (GB) reflection.

for every propagation mode. For the ℓ -th propagation mode, the rays departing from the BS with specific AoD ϑ_ℓ reach the SAT experiencing a different array gain and clutter loss. Given the geometrical stochastic parameters Θ , the interference power at the SAT from the q -th BS can be evaluated by adopting (2) in dB scale as

$$[I_q^\ell(\Theta)] = [P_T] + [G_a(\vartheta_\ell|\vartheta_k, \Theta)] + [G_c(\vartheta_\ell|\Theta)] + [\alpha_s], \quad (5)$$

where $[x]$ denotes the value of x in dB scale, $G_c(\vartheta_\ell|\Theta) = A_c^{-1}(\vartheta_\ell|\Theta)$ is the clutter gain, inverse of the clutter loss defined in (2). The corresponding PDF of $[I_q^\ell(\Theta)]$ is obtained as (6) (bottom of the page) by means of the *logarithmic convolution* [28]. The PDF of the interference power in linear scale, i.e. $\mathcal{P}(I_q^\ell|\Theta)$, can be easily converted from dB scale as indicated in [28]. Given the joint PDF of the geometrical parameters Θ , $\mathcal{P}(\Theta|\phi_s)$, we can write:

$$\mathcal{P}(I_q^\ell) = \mathbb{E}_\Theta [\mathcal{P}(I_q^\ell|\Theta)] = \int \dots \int \mathcal{P}(I_q^\ell|\Theta) \mathcal{P}(\Theta|\phi_s) d\Theta, \quad (7)$$

where $\mathbb{E}_z[x]$ is the expectation of x over z . Note that the probability distribution of the geometrical parameters $\mathcal{P}(\Theta|\phi_s)$ is conditioned to a given satellite azimuth ϕ_s , that is acquired for a given city or area, as detailed in Sec. VII. The analysis of the interference power is carried out using the CF of the $\mathcal{P}(I_q^\ell)$, defined hereafter as $\Phi_q^\ell(\omega) \triangleq \mathbb{E}\{e^{i\omega I_q^\ell}\}$. The usage of the CF is preferred in interference analysis [29]–[31], because it always exists when it is a function of a real-valued argument [32], and cumbersome convolution operations can be converted to simpler products. The aggregated interference from q -th BS to SAT, I_q , is the independent summation (in linear scale [33], [34]) over the

L possible interference modes, whose CF is achieved as

$$\Phi_q(\omega) = \prod_{\ell=1}^L \Phi_q^\ell(\omega). \quad (8)$$

This CF is used in Sec. IV for aggregation of interference coming from all BSs in a given region.

B. Geometry-based stochastic model of interference (GSMI)

The GSMI method is an alternative to SMI whenever the PDF of clutter gain $\mathcal{P}([G_c|\vartheta_\ell, \Theta])$ in (6) is not available. Typically, $\mathcal{P}([G_c|\vartheta_\ell, \Theta])$ is obtained by means of exhaustive and computationally intensive ray-tracing simulations, which could be unavailable in some cases, especially over large areas such as the SATFP. With GSMI, we assume that the interference at the SAT comes from a limited set of interference modes. These are the following: (i) direct path (DP); (ii) single-building (SB) reflection; (iii) double building (DB) reflection; (iv) ground reflection (GR); (v) ground and building (GB) reflection, while other reflections are neglected due to higher propagation losses. Herein, we denote the set of considered modes as $\mathcal{M} = \{DP, SB, DB, GR, GB\}$. The ℓ -th interference mode $\ell \in \mathcal{M}$ can occur with a certain probability $\mathcal{P}_\ell(\Theta)$, that depends on the system parameters Θ as well as on the BS type. Since micro BSs are assumed to be placed on the ground, they can experience *all* the interference modes, while for macro BS, located on the rooftop, SB and DB, typically do not occur. Note that, one or more interference modes might occur simultaneously, and thus we have

$$0 \leq \sum_{\ell=1}^{|\mathcal{M}|} \mathcal{P}_\ell(\Theta) \leq |\mathcal{M}|. \quad (9)$$

Appendix IX reports the derivation of $\mathcal{P}_\ell(\Theta)$ and further information.

Unlike the SMI method, where the possible interference modes L is usually large, here the interference is limited to only 5 contributions (3 in case of rooftop BS). The average probability of occurrence of the ℓ -th mode can be computed as

$$\bar{\mathcal{P}}_\ell = \mathbb{E}_\Theta [\mathcal{P}_\ell(\Theta)]. \quad (10)$$

The interference power and its PDF in each interference mode ℓ from q -th BS, $\mathcal{P}(I_q^\ell)$, is achieved with (5), (6) and (7) by removing the clutter gain and its PDF. However, it must be noted that, since every interference mode considered in the GSMI method has a specific occurrence probability, the PDF of the interference is conditioned to the occurrence of the corresponding ℓ -th mode.

Thus, this difference can be modeled by slightly modifying (8), yielding

$$\Phi_q(\omega) = \prod_{\ell=1}^{|\mathcal{M}|} (\Phi_q^\ell(\omega))^{\bar{\mathcal{P}}_\ell}. \quad (11)$$

This modification is justified in Sec. IV when aggregating the interference coming from all BSs in a given region.

IV. Aggregation of Multiple BS

The interference power generated by a single BS is then aggregated over multiple BS such as over a city, or a large geographical region (e.g., the whole SATFP).

A. Aggregation over a city

The first aggregation step is to consider a whole area of a city S . The CF of the aggregated interference power at SAT from all the BSs (either macro or micro) is computed as

$$\Phi_I(\omega) = \begin{cases} \prod_{\ell=1}^L (\Phi_q^\ell(\omega))^Q, & \text{SMI.} \\ \prod_{\ell=1}^{|\mathcal{M}|} (\Phi_q^\ell(\omega))^{\bar{\mathcal{P}}_\ell Q}, & \text{GSMI.} \end{cases} \quad (12)$$

where $Q = S\rho\lambda F_T$ is the effective average number of BSs in the city, λ is the density of the macro/micro BSs, and ρ is the BS power loading factor based on the ITU recommendation [21] as the percentage ρ of all the BSs considered to be working at full power with maximum Tx power, and F_T is the BS TDD activity factor. Model (12) endorses that in the GSMI method, every interference mode occurs on average $\bar{\mathcal{P}}_\ell Q$ times, which is the rationale behind $\bar{\mathcal{P}}_\ell$ in (11).

The general aggregation rule (12) can be specialized to derive the CF in more specific cases, i.e., differentiating between different BS types (macro and micro) and UE locations (indoor vs. outdoor). The BS type affects the interference mostly through the height h_{BS} , which changes from macro to micro and affects the PDF of the array gain. Similar behavior is expected for the UE location (described by average UE height h_{UE}), as UEs located outdoor have $h_{UE} \approx 0$ while indoor UEs may have a much higher height from the ground. These assumptions affect the array gain and clutter loss. For example, let us consider the case of micro BSs, and assume that all the UEs are indoor. In this case, we have a constant BS height h_{BS} m by assumption (see Sec. II), and the UE is bound to the building height h as $0 < h_{UE} < h$. The former term influences directly the clutter loss $A_c(\vartheta_\ell|\Theta)$ (see Sec. VI), while the second indirectly affects the array gain, defining a specific AoD toward the k -th UE, ϑ_k . We denote the aggregated interference under these assumptions as $I_{m,i}$ and its CF with $\Phi_I^{m,i}(\omega)$. The table I summarizes the four different interference contributions over an entire city. Let $0 \leq \beta \leq 1$ be the fraction of outdoor

$$\mathcal{P}([I_q^\ell|\Theta]) = \mathcal{P}([P_T]) * \mathcal{P}([G_a|\vartheta_\ell, \Theta]) * \mathcal{P}([G_c|\vartheta_\ell, \Theta]) * \mathcal{P}([\alpha_s]). \quad (6)$$

TABLE 1: Interference contributions

BS Type	UE Type	Notation
Micro BS	Indoor	$I_{m,i}$ and $\Phi_I^{m,i}(\omega)$
Micro BS	Outdoor	$I_{m,o}$ and $\Phi_I^{m,o}(\omega)$
Macro BS	Indoor	$I_{M,i}$ and $\Phi_I^{M,i}(\omega)$
Macro BS	Outdoor	$I_{M,o}$ and $\Phi_I^{M,o}(\omega)$

UEs and $1 - \beta$ be the fraction of indoor UEs. The overall CF of the aggregated interference power is

$$\Phi_I(\omega) = \left(\Phi_I^{m,o}(\omega) \Phi_I^{M,o}(\omega) \right)^\beta \times \left(\Phi_I^{m,i}(\omega) \Phi_I^{M,i}(\omega) \right)^{1-\beta}. \quad (13)$$

Note that all of the micro and macro BSs coexist simultaneously, while a fraction of UEs is indoor/outdoor. The corresponding PDF $\mathcal{P}(I)$ is computed as the inverse Fourier transform of the CF as

$$\mathcal{P}(I) = \frac{1}{2\pi} \int_{-\infty}^{\infty} \Phi_I(\omega) e^{i\omega I} d\omega. \quad (14)$$

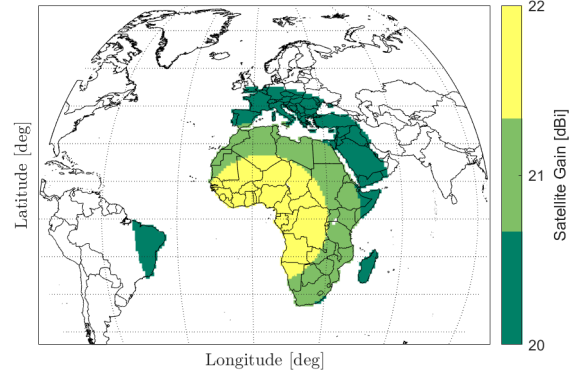
In practice $\mathcal{P}(I)$ is evaluated using the Gil Pelaez theorem of inversion [35], which can be carried out numerically [36].

B. Aggregation over the SATFP

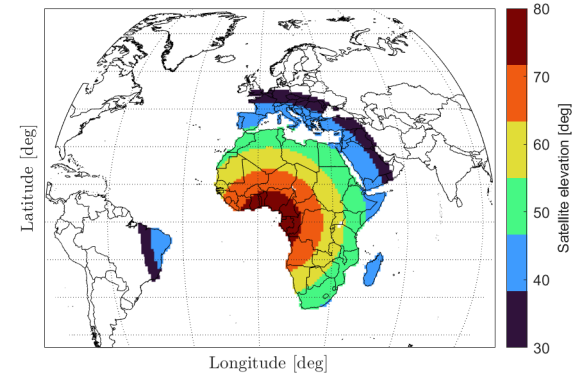
In case the aggregation area is larger than a single city, different locations on Earth's surface see the SAT under different elevation angles. This causes the interference contribution from the same BS model to be different based on latitude and longitude location [12]. To obtain the total aggregated interference, we first identify the regions that share similar link budget parameters towards the SAT, i.e., the same elevation angle and the same SAT antenna gain. These regions are called Geographic Clusters (GC).

Let us consider the example of a SAT occupying an orbital location (0N, 5E) in a GEO orbit and having the uplink antenna pointing at Nadir. Also, assume that the locations on Earth's surface are discretized by defining a tessellation of pixels of 1 deg along latitude and longitude. Fig. 5a shows the pixels inside the 3 dB SATFP assuming the antenna pattern model as defined in [37], with SAT gain G_s quantized in steps of 1 dB. The maximum gain and 3 dB beamwidth (22 dBi, and 15° respectively) are taken from ITU WP4 discussions and, assuming a parabolic antenna mounted on the satellite [38].

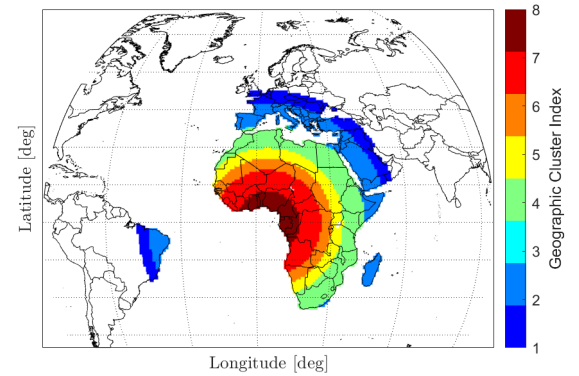
Assume that the set of GCs are $\mathcal{C} = \{C_1, C_2, \dots, C_v, \dots, C_\Upsilon\}$, where C_v denotes the v -th GC. The number of GCs is $|\mathcal{C}| = \Upsilon$. Now, the GCs inside SATFP will observe the SAT under different angles identified by azimuth and elevation pairs $\vartheta_s^v = (\phi_s^v, \psi_s^v)$, as depicted in Fig. 5b. Since the effect of the azimuth, ϕ_s^v is averaged out due to the fact that the BSs are assumed



(a)



(b)



(c)

FIGURE 5: (a) SAT antenna aperture gain 3 dB footprint; (b) elevation angle of SAT as seen from Earth; (c) geographic clusters obtained with selected G_s and ψ_s resolution.

to be randomly oriented throughout a large region (see Sec. V), only the impact of the SAT elevation is of interest. In Fig. 5b, the elevation angle of the SAT seen from Earth is depicted for each pixel with an angle quantization of 10 deg. Each GC can thus be represented as a unique pair (G_s^v, ψ_s^v) . The GCs obtained with the selected resolution are reported in Fig. 5c.

To compute the aggregated interference coming from the SATFP, for each GC we find the CF of its interference

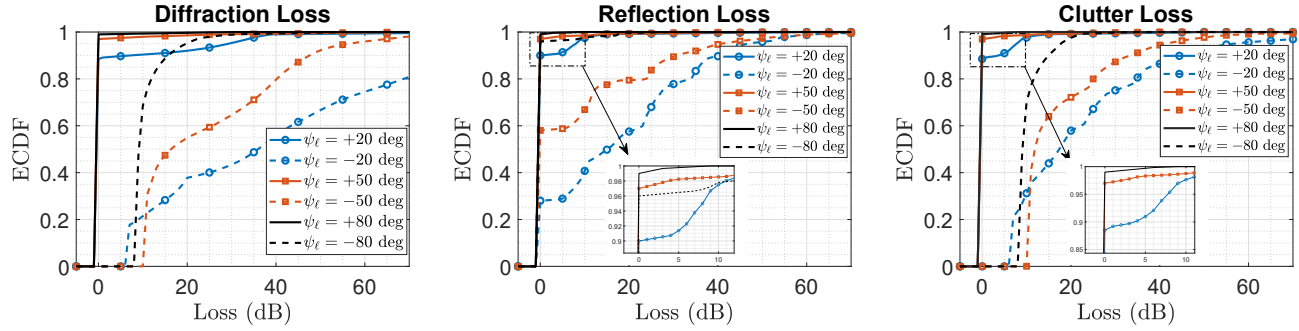


FIGURE 6: Empirical CDF (ECDF) of diffraction loss, reflection loss and clutter loss for the SAT elevation angles $\psi_s \in \{20, 50, 80\}$ deg for positive and negative modes, with BS height $h_{BS} = 6m$, for the city of Milan using the method in [39], [40].

contribution following the procedure detailed in Sec. III. Then we aggregate the CFs of all the GCs to find the overall result as

$$\Phi_{FP}(\omega) = \prod_{v=1}^{\Upsilon} \Phi_v(\omega) \quad (15)$$

where $\Phi_v(\omega)$ is the CF of interference from the v -th GC, computed with (13), using the corresponding SAT Rx gain on each GC G_s^v and the average number of BSs in the v -th GC $Q_v = \lambda \rho F_T R_a R_b S_v$. The latter is the product of the GC area S_v , the average density of the macro BSs λ , the BS loading factor ρ , TDD activity factor F_T , while R_a and R_b are parameters defined by ITU [27], to establish a bond between amounts of BS and large-scale land areas in the order of SATFP, where R_b is the percentage of built area, and R_a is the percentage of the area from a certain type, e.g., urban, suburban, and etc. Here we consider urban area type.

C. Interference protection criterion

Given the interference power I and signal bandwidth B , the interference protection criterion, is based on the INR defined as [41]:

$$\text{INR} = \frac{I}{BN_0}, \quad (16)$$

where $N_0 = K_B T_{\text{sys}}$ is the noise PSD with K_B as the Boltzmann constant and T_{sys} is the SAT Rx system temperature [42]. The SAT is protected from interference whenever interference threshold criterion $\text{INR} \leq \text{INR}_{th}$, with INR_{th} being a threshold specified by satellite regulators. In [43], the T_{sys} for a geostationary SAT is given for mmW in the range of 400 – 950 K depending on different parameters, while the calculations in [10], demonstrate system thermal noise of around 800 K in the C-band.

V. Stochastic Array Gain

This section details the modeling of the array gain $G_a(\vartheta|\vartheta_k, \Theta)$ and its PDF. We consider generic rectangular panels for each BS sector, each configured with N_V vertical

and N_H horizontal antennas. The equivalent isotropically radiated power (EIRP) is therefore defined as

$$\text{EIRP} = \frac{P_T N_V^2 N_H^2}{\eta}, \quad (17)$$

where η is the sub-array size (number of antennas connected to a single RF chain) in a hybrid digital-analog antenna array, and the Tx power P_T , is related to a single RF chain (i.e., a single power amplifier (PA)) [20], [21], while $\eta = 1$ corresponds to a fully digital antenna array. A feeder loss can be added to further reduce the effective EIRP as indicated in [44]. The horizontal and vertical gains assigned toward a generic azimuth ϕ and elevation ψ steering toward the k -th UE are

$$G_H(\phi|\phi_k) = |\mathbf{b}^H(\phi_k - \varrho)\mathbf{a}(\phi - \varrho)|^2 D_H(\phi - \varrho), \quad (18)$$

$$G_V(\psi|\psi_k) = |\mathbf{b}^H(\psi_k)\mathbf{a}(\psi + \psi_{\text{tilt}})|^2 D_V(\psi + \psi_{\text{tilt}}), \quad (19)$$

where: (i) $D_H(\phi)$ and $D_V(\psi)$ are the horizontal and vertical element directivity gains [45], [46], respectively, (ii) $\mathbf{a}(\phi) \in \mathbb{C}^{N_H \times 1}$ and $\mathbf{a}(\psi) \in \mathbb{C}^{N_V \times 1}$ are the horizontal and vertical ULA response vectors, respectively, (iii) $\mathbf{b}(\phi) \in \mathbb{C}^{N_H \times 1}$ and $\mathbf{b}(\psi) \in \mathbb{C}^{N_V \times 1}$ are the conventional horizontal and vertical beamforming, \mathbf{b}^H indicates the hermitian of vector \mathbf{b} , and ϱ is the orientation of the serving BS panel that is perceived by the SAT as $\varrho \sim U[0, 2\pi]$. Note that ϱ corresponds to any BS panel that observes the target azimuth ϕ within the electromagnetic (EM) shielding limit while serving the k -th UE, as $|\phi_k - \varrho| \leq \phi_{sh}$, where $\phi_{sh} = 60$ deg. With such an assumption, it is apparent that only one of the panels of the macro BS is capable of interfering with ϕ while serving a UE at ϕ_k . In the case of micro BS, depending on the number of the BSs and their orientations, one or multiple BSs might be interfering. The total gain is

$$G_a(\vartheta|\vartheta_k, \Theta) = G_V(\psi|\psi_k) G_H(\phi|\phi_k). \quad (20)$$

The corresponding array gain for ℓ -th interference mode with AoD ϑ_ℓ is denoted as $G_a(\vartheta_\ell|\vartheta_k, \Theta)$, that for the direct BS-SAT link would be $G_a(\vartheta_s|\vartheta_k, \Theta)$. The PDF of the array gain $\mathcal{P}(G_a|\vartheta_\ell, \Theta)$ is achieved by Monte-Carlo simulations,

given the random ϑ_k . This PDF is for the array gain toward a single UE, while the number of the served UEs affects the Tx power and the BS loading factor, rather than the array gain. Note that the random AoD of the k -th UE ϑ_k , is inherently a function of environment parameters Θ , as it depends on the cell size, random 2D position of the UEs within the cell, the distribution of the UEs height, and the distribution of the BS height.

VI. Stochastic Clutter Loss

Clutter is the term herein used to indicate objects that are on the Earth's surface, but are not the terrain itself, i.e. buildings and vegetation. Clutter loss $A_c(\vartheta_\ell|\Theta)$ consists of reflection loss $A_r(\vartheta_\ell|\Theta)$ and diffraction loss $A_d(\vartheta_\ell|\Theta)$, properly combined as indicated in [23].

Quantifying clutter loss is not trivial, since it is strongly dependent on both environment and geometry of the link of interest. The target AoD also plays a crucial role [47], [48]. One possible approach is to use a ray tracer to evaluate clutter loss via deterministic simulation, but the computational load makes this method applicable to limited areas only, yielding site-specific results that are not general enough [47]. As previously mentioned, ITU recommendation [23] contains guidelines to perform stochastic Monte Carlo simulation of clutter loss statistics, making use of environment geometrical data and stochastic geometry to evaluate the CDF of clutter loss at a given elevation angle ψ_s . Some of the stochastic parameters of the environment that serve as the input for this method are BS height, the material of the buildings/ground, and some specific percentiles of the inter-building distances and buildings' height.

Although the statistical nature of the approach in [23] is very much suited to our model, there are some limitations that can affect the applicability of this model: the model is not considered valid below 10 GHz, a limited number of reflections and diffraction are considered (up to two), the reflection coefficients are not dependent on angles of incidence and polarization. Furthermore, the main drawback is that this method is designed for only the direct BS-SAT link, and it does not provide distinct clutter loss statistics for different interference modes. This is while the SMI method require a distinct clutter loss $A_c(\vartheta_\ell|\Theta)$ corresponding to the ℓ -th propagation mode. In this regard, one could resort to the model proposed in [39], [40] as an extension of [23], where the aforementioned limitations are overcome, considering *positive* and *negative* interference modes. Positive modes are all the modes that leave the BS upward with elevation $+\psi_s$ and negative modes are all the modes that leave the BS downward with elevation $-\psi_s$, i.e. ground reflection modes. Fig. 6 shows the clutter-loss, diffraction-loss and reflection-loss, given the extracted geometrical statistics of Milan, when the BS is located at $h_{BS} = 6\text{m}$ height.

Remark: Being more specific regarding diffraction and reflection, it can be understood that the GSMI method, in fact, mimics the effect of diffraction loss, in a hard decision

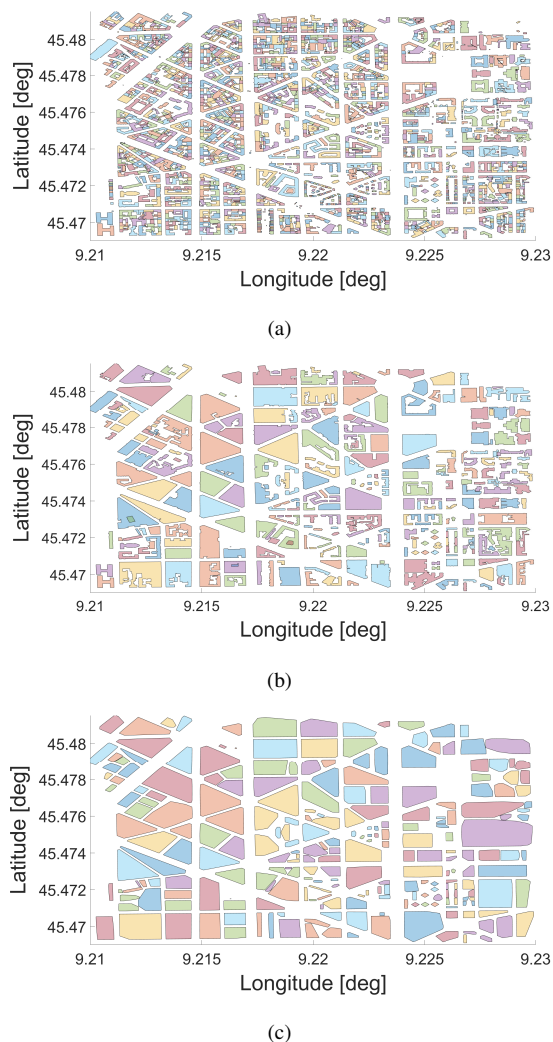


FIGURE 7: Dataset processing chain: (a) original dataset (city of Milan), (b) merging process, (c) convex shape approximation. The convexified polygons are used for extracting the necessary geometrical data.

manner, i.e., a ray is in line-of-sight (LOS) mode or fully blocked in a stochastic manner. However, in some cases, reflection loss is dominant as seen in Fig. 6. Thus, in order to take the reflection loss into account (if it is available), one can repeat the same procedures of GSMI method, by replacing $G_c(\vartheta_\ell|\Theta)$ and $\mathcal{P}(G_c|\vartheta_\ell, \Theta)$ with reflection gain $G_r(\vartheta_\ell|\Theta) = A_r(\vartheta_\ell|\Theta)^{-1}$ and its PDF $\mathcal{P}(G_r|\vartheta_\ell, \Theta)$ in relations (5) and (6), respectively.

VII. Geometrical Statistics

As shown in Section II, the set of geometrical parameters Θ is required to calculate the interference power. These parameters affect both the array gain and clutter loss (see Sec. V and Sec. VI). Furthermore, they are necessary to compute the occurrence probability $\mathcal{P}_\ell(\Theta)$ in the GSMI method as (10). These geometrical statistics used are extracted using

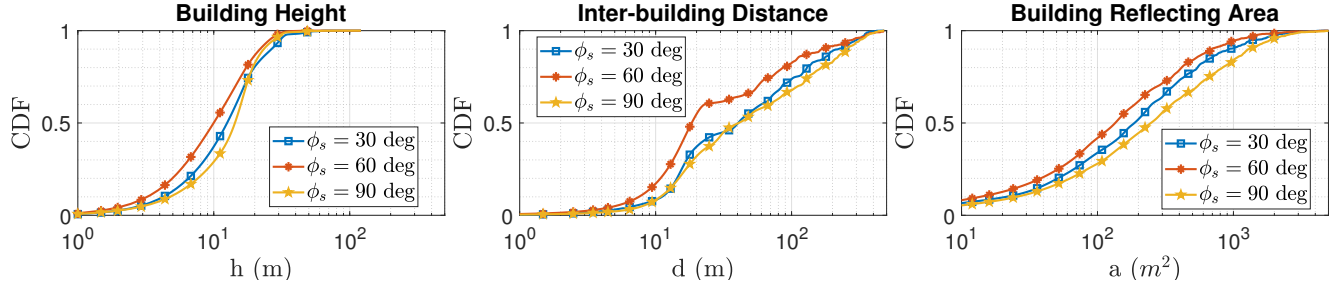


FIGURE 8: CDF of the geometrical parameters, extracted for city of Milan, given $\phi_s = \{30, 60, 90\}$ deg, that serve as raw input data for the calculation of the ECDF of array gain and the clutter loss models [23], [39], [40].

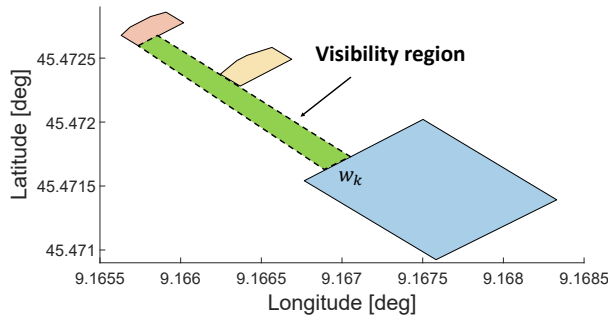


FIGURE 9: Inter-distance between the buildings having 2 parallel walls. The green area identifies the visibility region. Note that the buildings in yellow acts as an obstacle reducing the visibility region between the red and blue buildings.

a pseudo-3D or 2.5D approach [49], [50], where the 3D geometry is split into 2D cross-sections along the SAT azimuth ϕ_s . The city of Milan is taken as a reference, and we generate (i) the PDFs of the buildings' heights, (ii) the PDFs of the reflection area of each building's facade, and (iii) the PDFs of buildings' inter-distance (i.e., streets' widths), each on a regular azimuth grid with quantization step of $\Delta\phi = 5$ deg, using relevant public datasets with further processing [51]. Fig. 7a shows an exemplary portion of Milan from the original dataset, where each polygon defines a specific detail of a building with a particular height. Such details are not required, as we are interested in representing only the external buildings' facades, and some merging processes can be applied to reduce the complexity of the environment while maintaining useful geometrical information. The convexification process is shown in Fig. 7a to 7c, where the final convex polygons are associated with average heights and widths, retrieved for each merged building. Although not reported here, it can be shown that the merging-plus-convex approximation of the buildings' geometry preserves the facades' area.

From the simplified dataset, we generate the PDFs for each SAT azimuth angle ϕ_s . The buildings' heights are discretized at $\Delta h = 5$ m and the PDF $\mathcal{P}(h|\phi_s)$ is derived from the histogram.

Each entry of the histogram is a weighted sum of all the building's facades of height h_i perpendicular to the azimuth satellite direction ϕ_s , (i.e., that can effectively contribute to the clutter loss)

The PDF of the buildings' reflecting area $\mathcal{P}(a|\phi_s)$ is evaluated similarly, by using the histogram of occurrence of a certain reflection area a , discretized with a step of $\Delta a = 20$ m². Differently, the PDF of the buildings' inter-distance is weighted by the effective *visibility region* (or visibility polygon), which in the context of computational geometry is defined as the 3D region between adjacent buildings with parallel facades without obstacles [52], as illustrated in Fig. 9. The PDF is again approximated as

$$\mathcal{P}(d|\phi_s) \approx \frac{\mathbf{d}(\phi_s)}{\sum_{j=1}^{N_h} [\mathbf{d}(\phi_s)]_j}, \quad (21)$$

where $\mathbf{d}(\phi_s)$ is the inter-distance histogram quantized with step $\Delta d = 5$ m, but the j -th histogram element $[\mathbf{d}(\phi_s)]_j$ is now computed as

$$[\mathbf{d}(\phi_s)]_j = \sum_{k \in \mathcal{W}_j(\phi_s)} w_k h_k, \quad (22)$$

where w_k is the width of the visibility region of two adjacent buildings with parallel facades and h_k is the average height of the two involved facades. The set $\mathcal{W}_j(\phi_s)$, therefore, spans all the pairs of parallel facades at distance d_j and perpendicular to ϕ_s . Fig. 8 shows the distribution of building's height h , inter-building distance d , and buildings' reflection area a , given some exemplary SAT azimuth $\phi_s = \{30, 60, 90\}$ deg.

VIII. Numerical Results

This section shows the numerical aggregated interference power density for the city of Milan and the SATFP.

A. Simulation setup

The BS arrangement is the same depicted in Fig. 3 (Section II). For each macro cell, we consider 3 single-sector micro BS, for a total of 9 micro BS for each macro BS. Micro BSs are placed at $h_{BS} = 6$ m [16], [21], while macro BSs are at $h_{BS} = \max(h, 6)$ m, where h is the height of the tallest building in the 3 macro cells pertaining to the same macro

TABLE 2: Array configurations

	Config. 1		Config. 2	
	macro	micro	macro	micro
N_H	8	4	8	8
N_V	8	8	16	8
η	1	1	2	2
A_f (dB)	3	3	3	3
P_T (dBm)	25	19	22	16
EIRP (dBm)	58	46	58	46
ψ_{3dB} (deg) [45]	65	65	65	65
ϕ_{3dB} (deg) [45]	65	65	65	65
ψ_{tilt} (deg)	-10	-10	-10	-10
G_e (dBi) [45]	8	8	8	8

BS. The distributions of height of the buildings h and inter-building distance d are obtained as in Sec. VII (see Fig. 8) for $\phi_s = 45$ deg. The building-BS distance d_1 (see Fig. 4) is not known, thus, it is assumed to be uniform in d : $d_1 \sim U[0, d]$. It can be shown that if the BS is placed symmetrically w.r.t. the center of the road ($d_1 = d/2$), the results in terms of aggregated interference power do not appreciably change.

The macro cell radius considered is $d_c = 300$ m [21] and the macro BS density is therefore $\lambda = 1/(3S_c)$, where S_c is the macro cell's area. The micro cell radius is assumed to be $d_m = d_c/4$. Each micro BS serves UEs within d_m , while the rest are served by the macro BS.

The UEs are considered to be randomly located either on the ground (outdoor UEs) and inside the buildings (indoor UEs), according to a 2D random distribution with spatial density λ_{UE} [UE/m²] (on the ground plane). Outdoor UEs are assumed to have a constant height $h_{UE} = 1.5$ meter. Indoor UEs' height is assumed to be $h_{UE} \sim U[1.5, h]$ meters, where h follows the distribution of the buildings' height. Table 2 shows the array configurations used for macro and micro BSs in this paper. The antenna element directivity model is based on [20], [45], with maximum element directivity gain G_e , vertical and horizontal fields of view of ψ_{3dB} and ϕ_{3dB} , respectively, and feeder loss A_f (see Table 2). Fig. 10, shows an example of the empirical CDF (ECDF) of the array gain for the macro BS toward ϑ_ℓ , averaged over the distribution of the height of the buildings and the height of the UEs, when serving an indoor UE with array configuration 1 of table 2. It can be noticed that interference modes characterized by $\psi_\ell < 0$ (i.e., reflections from the ground) are characterized by a higher array gain, and, consequently, a larger interference contribution as the

TABLE 3: Simulation parameters

Parameter Name	Parameter	Value
SAT azimuth	ϕ_s (deg)	45
central frequency	F_c (GHz)	6
SAT distance	d_s (Km)	35000
path loss	A_p (dB)	199
bandwidth	B (MHz)	100
Macro cell radius	d_c (m)	300
SAT Rx temperature [10]	T_{sys} (Kelvin)	800
threshold INR at 80% [27]	INT_{th} (dB)	-10.5
polarization loss	A_{pol} (dB)	3
BS loading factor [27]	ρ	20%
TDD activity factor [27]	F_T	75%
Ratio of urban area type [27]	R_a	5%, 10%
Ratio of built-up areas [27]	R_b	1%

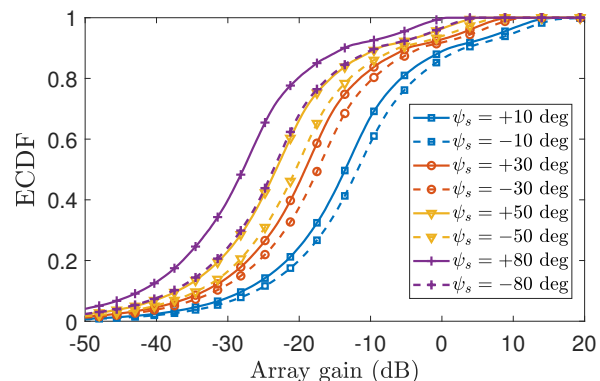


FIGURE 10: Empirical CDF (ECDF) of the Array gain for a macro BS, serving UEs inside the buildings, distributed vertically uniform over the height of the building, using the array configuration 1, in Table 2.

BS is tilted towards the ground. Table. 3 summarizes other relevant simulation parameters.

B. Aggregated interference from the city of Milan

Figure 11 shows the CDF of the aggregated interference power density, using the SMI method with array configuration 1 (Table 2). Given the area of the city of Milan $S_{\text{Milan}} = 181.76$ km², the equivalent number of BSs with maximum power is $Q = 155.5$. It can be observed that the INR based on the aggregated interference coming from a city of Milan size is much lower than $\text{INR}_{th} = -10.5$ dB. It can be seen that, as the elevation angle decreases, the interference

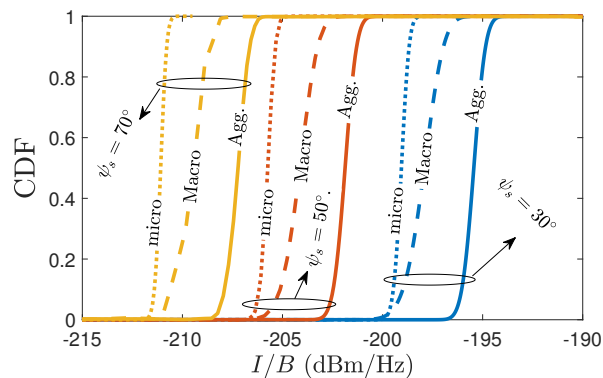


FIGURE 11: CDF of the interference PSD using SMI method for the city of Milan, with array configurations 1 of Table 2, and exemplary SAT gain $G_s = 20$ dB.

from macro BSs becomes dominant w.r.t. the one from micro BSs. The reason is that, for positive interference modes, micro BSs are typically affected by higher clutter-loss due to their lower height, while macro BSs are typically placed on top of buildings and experience minimal clutter-loss loss at high satellite elevation angles such as $\psi_s = 70$ deg. When the satellite elevation angle decreases, the clutter-loss also affects macro BSs. Notice that, if the interference contribution of macro and micro BS is exactly the same, the median of the aggregated interference curve would be approximately 3 dB higher. Differently, in case one contribution (either from macro or micro BSs) is dominant, the aggregated curve would be superposed with the dominant one. It must be noted that the distribution of the aggregated interference for the macro and micro BS cases may be correlated, as both the array gain PDF and clutter loss PDF depend on the geometric statistics, which in turn pertain to the same city.

C. Aggregated interference of SATFP

In order to encompass the interference from the SATFP, we follow the methodology introduced in Sec. B. The corresponding specifications of each GC are shown in Table 4. The values of $R_a = 5\%$ and $R_a = 10\%$ are chosen according to [53] and [27], respectively. The average loading factor $\rho = 20\%$ corresponds to typical values of coexistence studies when the area under study is a large region consisting of hundreds of BSs or more [27].

Figures 12a and 12b show the median value of the INR using the array configuration 1, for 8 GCs and the whole SATFP (see Section B), with SMI and GSMI methods. It can be seen that with $R_a = 5\%$, the INR is well below the threshold INR_{th} , while only for extremely dense deployments with $R_a = 10\%$, would yield an INR level close to INR_{th} . Notice that the SMI method is the baseline model and GSMI is an approximate method that overestimates the interference w.r.t. the SMI by approx. 2 dB. One way to reduce the aggregated interference power is to increase the number of array antennas on the vertical plane while

TABLE 4: Specifications of footprint GCs

#GC (v)	G_s^v (dBi)	S_v (km^2)	ψ_s^v (deg)
1	20	3 812 552	30
2	20	6 654 033	40
3	21	30 088	40
4	21	9 203 759	50
5	21	5 104 969	60
6	22	4 632 108	60
7	22	6 869 836	70
8	22	2 605 246	80

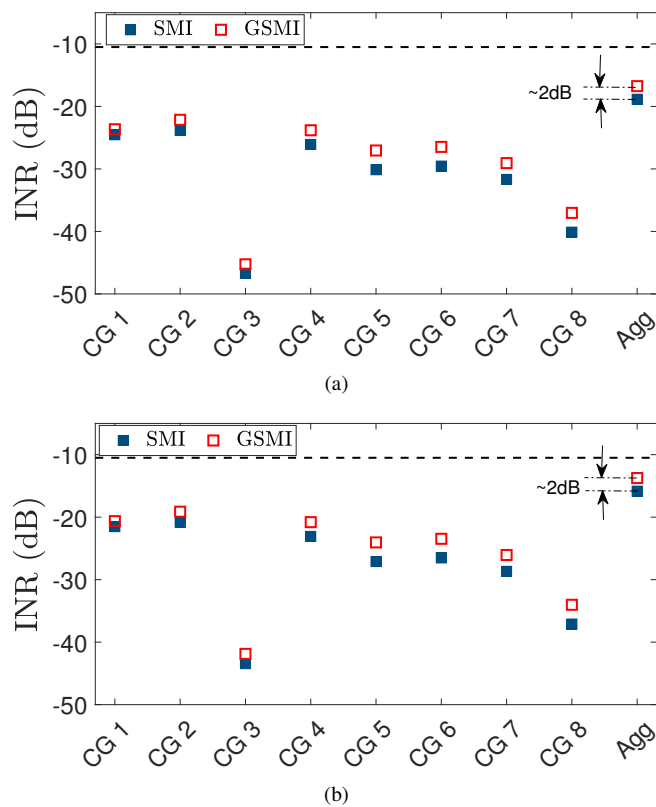


FIGURE 12: INR at 80 percentile for different GCs and the aggregated of SATFP, for: a) $R_a = 5\%$; b) $R_a = 10\%$ (array configuration 1).

keeping constant EIRP and preserving the quality of the U6G service. The consequent reduction of sidelobes' level diminishes the interference at SAT. Figure 13 shows the INR for the two array configurations in Table 2. The 80 percentile of the INR is decreased by more than 4 dB when using the antenna array configuration 2, i.e., double the antennas on the vertical plane of the macro BS. In this latter case, even

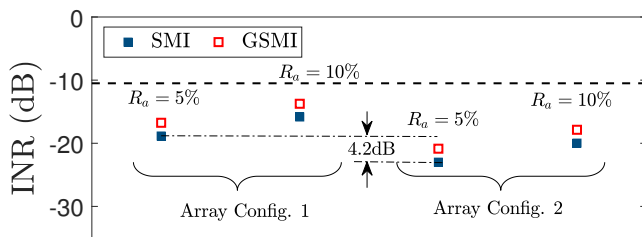


FIGURE 13: INR of SATFP at 80 percentile, comparing the first and second set of BS array configurations.

the extremely dense deployments with $R_a = 10\%$ would be well below the INR_{th} . We remark that, in addition to antenna array design methods, other valid solutions to reduce U6G interference can be considered, such as elevation domain shielding, irregular array design, improved beamforming techniques, usage of highly directive elements etc. [54]–[57]. The detailed discussion of these methods goes beyond the scope of the paper, and it is not treated here.

Here, the level of aggregated interference has been separately calculated for each GC, depending on the elevation of the SAT observed at that given region, and finally, the overall interference is calculated. This is more realistic and accurate than the method adopted in [12] where a constant SAT elevation is assumed everywhere. The numerical results are herein obtained using the statistics of the city of Milan since the statistics of each GC are not available. A more accurate estimation of the level of interference requires accurate knowledge of the distribution of geometrical parameters for every different region. The latter distributions can significantly vary across different cities and, furthermore, factors beyond geometrical parameters can also influence clutter loss and reflection coefficient, such as precipitation levels, temperature, snow coverage, vegetation coverage, and other environmental factors [40]. However, this does not affect the generality of the proposed stochastic method, that applies to any scenario (even operating at other frequencies) upon proper adjustment of geometrical parameters and propagation models.

As a final remark, we underline that the methodology adopted in this paper is suited to GEO SATs, due to their static nature. However, the proposed methods can be extended to low Earth orbit (LEO) and medium Earth orbit (MEO) SATs as well, with suitable adjustments. For instance, LEO and MEO SATs have a much less path-loss to/from ground and a higher INR threshold [58]. Moreover, low orbit SATs have a reduced SATFP compared to GEO ones. The dynamic nature of low orbit SATs is however, the main challenge for the extension of the present SMI and GSMI methods. The aggregated interference toward the SAT at a certain elevation would be different w.r.t another elevation, making it a function of time as well as azimuth-elevation. Such dynamic behavior has not been addressed

in other works involving LEO SATs [12]. The adaptation of SMI and GSMI to LEO and MEO SATs is not covered here.

IX. Conclusion

In this paper, we develop a SMI method to evaluate the aggregate interference power at GEO SATs in U6G band from a set of BSs belonging to an arbitrarily large geographical area. The SMI is based on the distributions of the array gain and the clutter (reflection and diffraction) loss, and it considers different interference modes such as direct path and reflections from buildings and ground. In addition, we propose a GSMI method to be used in the absence of the distribution of diffraction loss and/or reflection loss. We show, for typical parameters' values in the context of communications coexistence, that the interference power generated by U6G BSs toward GEO SATs in typical cases is below the tolerable interference thresholds set by ITU standards. Moreover, we discussed a possible solution to reduce the interference by proper modifications to the BS array design.

Acknowledgement

The research has been carried out in the framework of the Joint Lab between Huawei and Politecnico di Milano. The authors would like to acknowledge the enlightening discussions and clarifications with Prof. Carlo Riva on clutter loss models.

APPENDIX

Calculation of occurrence probabilities

The occurrence probability of the direct path between BS and SAT can be computed from basic geometrical considerations. Based on Fig. 14, the direct path exists whenever it is not blocked by building 2, thus when $h_2 < h_{BS} + d_2 \tan(\psi_s)$. Given the CDF of the buildings' height, defined as

$$F_h(h) = \int_0^h \mathcal{P}(\xi|\phi_s) d\xi,$$

where $\mathcal{P}(\xi|\phi_s)$ is detailed in Sec. VII. The occurrence probability of this interference mode is

$$\mathcal{P}_{DP} = F_h(h_{BS} + d_2 \tan(\psi_s)|\phi_s).$$

Other interference modes are similarly treated, with straightforward modifications, using the image method (see e.g., [59], [60]). The corresponding occurrence probabilities are not reported for brevity.

REFERENCES

- [1] G. Naik, J.-M. Park, J. Ashdown, and W. Lehr, "Next Generation Wi-Fi and 5G NR-U in the 6 GHz Bands: Opportunities and Challenges," *IEEE Access*, vol. 8, pp. 153 027–153 056, 2020.
- [2] Coleago Consulting, "The 6 GHz opportunity for IMT. 5G area traffic demand vs. area traffic capacity supply," Aug. 2020. [Online]. Available: <http://www.coleago.com/app/uploads/2020/09/The-6GHz-Opportunity-for-IMT-Coleago-1-Aug-2020-002.pdf>

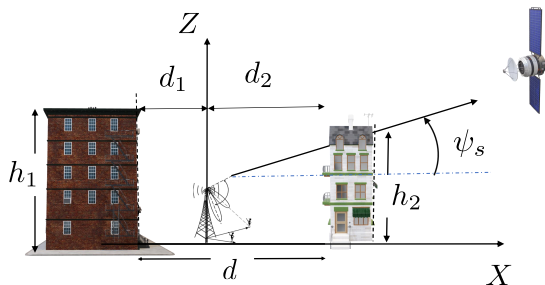


FIGURE 14: Side view of the direct path propagation mode

[3] US Federal Communications Commission, "Unlicensed Use of the 6 GHz Band, Report and Order and Further Notice of Proposed Rulemaking ET Docket No. 18-295; GN Docket No. 17-183," Dec. 2019. [Online]. Available: <https://www.federalregister.gov/documents/2020/05/28/2020-11320/unlicensed-use-of-the-6-ghz-band>

[4] Analysis Mason, "Discussion on the 6GHz opportunity for IMT," Dec. 2019. [Online]. Available: <https://www.analysismason.com/contentassets/2a36d000895f4700a2273d3bfee449bf/discussion-on-the-6-ghz-opportunity-for-imt.pdf>

[5] GSMA, "Estimating the mid-band spectrum needs in the 2025-2030 time frame." [Online]. Available: <https://www.gsma.com/spectrum/wp-content/uploads/2021/07/Estimating-Mid-Band-Spectrum-Needs.pdf>

[6] GSMA, "Vision 2030: Insights for Mid-band Spectrum Needs." [Online]. Available: <https://www.gsma.com/spectrum/wp-content/uploads/2022/07/5G-Mid-Band-Spectrum-Needs.pdf>

[7] L. Nan, G. Chunxia, and W. Dapeng, "Considerations on 6 GHz Spectrum for 5G-Advanced and 6G," *IEEE Communications Standards Magazine*, vol. 5, no. 3, pp. 5–7, 2021.

[8] L. Ippolito, "Radio propagation for space communications systems," *Proceedings of the IEEE*, vol. 69, no. 6, pp. 697–727, 1981.

[9] W. A. Hassan, H.-S. Jo, and A. R. Tharek, "The feasibility of coexistence between 5g and existing services in the imt-2020 candidate bands in malaysia," *IEEE Access*, vol. 5, pp. 14 867–14 888, 2017.

[10] Y. Li, A. Monti Guarnieri, C. Hu, and F. Rocca, "Performance and Requirements of GEO SAR Systems in the Presence of Radio Frequency Interferences," 2018.

[11] F. Guidolin, M. Nekovee, L. Badia, and M. Zorzi, "A study on the coexistence of fixed satellite service and cellular networks in a mmwave scenario," in *2015 IEEE International Conference on Communications (ICC)*, 2015, pp. 2444–2449.

[12] Y. Cho, H.-K. Kim, M. Nekovee, and H.-S. Jo, "Coexistence of 5G With Satellite Services in the Millimeter-Wave Band," *IEEE Access*, vol. 8, pp. 163 618–163 636, 2020.

[13] Y. Cho, H. Kim, D. K. Tetey, K.-J. Lee, and H.-S. Jo, "Modeling Method for Interference Analysis between IMT-2020 and Satellite in the mmWave Band," in *2019 IEEE Globecom Workshops (GC Wkshps)*, 2019, pp. 1–6.

[14] S. Liu, X. Hu, and W. Wang, *Frequency Sharing of IMT-2020 and Mobile Satellite Service in 45.5–47 GHz*, 01 2018, pp. 127–135.

[15] V. J. Richard Rudd, Selcuk Kirtay, "Coexistence of terrestrial and satellite services at 26 GHz," plumconsulting.co.uk, 2019.

[16] Z. Qian, T. Wang, Z. Fang, and T. He, "Sharing and compatibility studies of IMT systems with Earth Exploration-Satellite Service in 26 GHz frequency band," vol. 1087, p. 042021, sep 2018.

[17] G. Hattab, E. Visotsky, M. Cudak, and A. Ghosh, "Coexistence of 5g mmwave users with incumbent fixed stations over 70 and 80 ghz," in *2017 IEEE Globecom Workshops (GC Wkshps)*, 2017, pp. 1–5.

[18] ITU, "Final Acts WRC-15: World Radiocommunication Conference," 2015.

[19] ITU-R P.2108-1, "Prediction of clutter loss," Sep. 2021.

[20] ITU-R M.2101-0, "Modelling and simulation of IMT networks and systems for use in sharing and compatibility studies," Feb. 2017.

[21] ITU-R M.2292-0, "Characteristics of terrestrial IMT-Advanced systems for frequency sharing/interference analyses," Dec. 2013.

[22] ITU-R P.619-5, "Propagation data required for the evaluation of interference between stations in space and those on the surface of the Earth," Sep. 2021.

[23] ITU-R P.2402-0, "A method to predict the statistics of clutter loss for earth-space and aeronautical paths," Mar. 2017.

[24] ITU-R P.619-5, "Propagation data required for the evaluation of interference between stations in space and those on the surface of the Earth," Sep. 2021.

[25] Y. Banday, G. Rather, and G. R. Begh, "Effect of atmospheric absorption on millimeter wave (mmwave) frequencies for 5g cellular networks," *IET Communications*, vol. 13, 02 2019.

[26] Radiocommunication Study Groups, "Characteristics of terrestrial component of IMT for sharing and compatibility studies in preparation for WRC-23," SWG Sharing Studies, Jun. 2021.

[27] Annex 4.4 to Working Party 5D Chairman's Report, "Characteristics of terrestrial component of IMT for sharing and compatibility studies in preparation for WRC-23," Jun. 2021.

[28] J. Punt and D. Sparreboom, "Summing received signal powers with arbitrary probability density functions on a logarithmic scale," *Wireless Personal Communications*, vol. 3, pp. 215–224, 01 1996.

[29] R. Aghazadeh Ayoubi and U. Spagnolini, "Performance of Dense Wireless Networks in 5G and beyond Using Stochastic Geometry," *Mathematics*, vol. 10, no. 7, 2022.

[30] H. ElSawy, E. Hossain, and M. Haenggi, "Stochastic geometry for modeling, analysis, and design of multi-tier and cognitive cellular wireless networks: A survey," *IEEE Communications Surveys and Tutorials*, vol. 15, no. 3, pp. 996–1019, 2013.

[31] M. Z. Win, P. C. Pinto, and L. A. Shepp, "A mathematical theory of network interference and its applications," *Proceedings of the IEEE*, vol. 97, no. 2, pp. 205–230, 2009.

[32] E. Lukacs, "A survey of the theory of characteristic functions," *Advances in Applied Probability*, vol. 4, no. 1, pp. 1–38, 1972. [Online]. Available: <http://www.jstor.org/stable/1425805>

[33] S. Schwartz and Y. Yeh, "On the distribution function and moments of power sums with log-normal components," *Bell System Technical Journal*, vol. 61, 09 1982.

[34] N. Beaulieu, A. Abu-Dayya, and P. McLane, "Comparison of methods of computing lognormal sum distributions and outages for digital wireless applications," 06 1994, pp. 1270 – 1275 vol.3.

[35] J. Gil-Pelaez, "Note on the inversion theorem," *Biometrika*, vol. 38, no. 3/4, pp. 481–482, 1951. [Online]. Available: <http://www.jstor.org/stable/2332598>

[36] V. Witkovský, "Numerical inversion of a characteristic function: An alternative tool to form the probability distribution of output quantity in linear measurement models," *ACTA IMEKO*, vol. 5, p. 32, 11 2016.

[37] ITU-R S.672-4, "Satellite antenna radiation pattern for use as a design objective in the fixed-satellite service employing geostationary satellites," Sep. 1997.

[38] S. J. Orfanidis, "Electromagnetic Waves and Antennas," 2016. [Online]. Available: <https://www.ece.rutgers.edu/~orfanidi/ewal/>

[39] C. G. Riva, L. Luini, A. Panzeri, F. Morandi, L. Resteghini, D. De Donno, C. Mazzucco, and R. Lombardi, "A clutter loss model for satellite communication systems," *Electronics*, vol. 12, no. 1, 2023. [Online]. Available: <https://www.mdpi.com/2079-9292/12/1/186>

[40] ITU-R, "A method to predict the statistics of clutter loss for earth-space and aeronautical paths", Annex 16 to the Working Party 3K Chairman's Report (Document 3K/264-E)," Jun. 2022. [Online]. Available: https://www.itu.int/dms_ties/itu-r/md/19/wp3k/c/19-R-WP3K-C-0264!N16!MSW-E.docx

[41] ITU-R S.1323-1, "Maximum permissible levels of interference in a satellite network," 1997-2000.

[42] J. Kadish and W. T. East, "Satellite Communications Fundamentals". Artech House, 2000.

[43] ITU WRC-19, "FSS Technical Parameters for Sharing Studies, Agenda Item 1.13 and 1.14." Jun. 2021. [Online]. Available: <https://www.itu.int/md/R15-WP4A-C-0504/en>

[44] ITU-T Series K Supplement 16, "Protection against interference: Electromagnetic field compliance assessments for 5G wireless networks," Mar. 2017.

[45] 3GPP ETSI TR 138 900, "Study on channel model for frequency spectrum above 6 GHz (version 14.2.0 Release 14)," Jun 2017.

[46] M. Rebato, L. Resteghini, C. Mazzucco, and M. Zorzi, "Study of Realistic Antenna Patterns in 5G mmWave Cellular Scenarios," in *2018 IEEE International Conference on Communications (ICC)*, 2018.

- [47] P. Valtr, J. Zeleny, P. Pechac, and M. Grabner, "Clutter loss modelling for low elevation link scenarios," *International Journal of Antennas and Propagation*, vol. 2016, pp. 1–4, 03 2016.
- [48] K. Ishitomo, S. Ichitsubo, H. Omote, and T. Fujii, "Elevation angle characteristics of clutter loss in urban areas for mobile communications," 2019, pp. 1–4.
- [49] T. Alwajeeh, P. Combeau, R. Vauzelle, and A. Bounceur, "A high-speed 2.5d ray-tracing propagation model for microcellular systems, application: Smart cities," in *2017 11th European Conference on Antennas and Propagation (EUCAP)*, 2017, pp. 3515–3519.
- [50] Z. Liu, L.-X. Guo, and W. Tao, "Full automatic preprocessing of digital map for 2.5d ray tracing propagation model in urban microcellular environment," *Waves in Random and Complex Media*, vol. 23, 08 2013.
- [51] Comune di Milano, "Milano geo portale," <https://geoportale.comune.milano.it/sit/open-data/>.
- [52] H. El Gindy and D. Avis, "A linear algorithm for computing the visibility polygon from a point," *Journal of Algorithms*, vol. 2, no. 2, pp. 186–197, 1981. [Online]. Available: <https://www.sciencedirect.com/science/article/pii/0196677481900195>
- [53] ITU, "Liaison statement to Task Group 5/1 - Spectrum needs and characteristics for the terrestrial component of IMT in the frequency range between 24.25 GHz and 86 GHz," Jun 2017. [Online]. Available: <https://www.itu.int/md/R15-TG5.1-C-0036/en>
- [54] L. Resteghini, R. Flamini, C. Massagrande, V. Verri, C. Mazzucco, and R. Lombardi, "Irregularly clustered antenna array: A prototype for mmw 5g base station," in *2021 IEEE International Symposium on Antennas and Propagation and USNC-URSI Radio Science Meeting (APS/URSI)*, 2021, pp. 793–794.
- [55] L. Musumeci, "Advanced signal processing techniques for interference removal in satellite navigation systems," Ph.D. dissertation, 01 2014.
- [56] J. R. Sklar, "Interference mitigation approaches for the global positioning system," 2003.
- [57] J. Jayasinghe, J. Anguera, and D. Uduwawala, "A high-directivity microstrip patch antenna design by using genetic algorithm optimization," *Progress In Electromagnetics Research C*, vol. 37, pp. 131–144, 02 2013.
- [58] ITU-R RS.2017-0, "Performance and Interference Criteria for Satellite Passive Remote Sensing," 2012. [Online]. Available: <https://www.itu.int/rec/R-REC-RS.2017/en>
- [59] I. Wald, "Realtime ray tracing and interactive global illumination," Ph.D. dissertation, 01 2004.
- [60] S. Tan and H. Tan, "A microcellular communications propagation model based on the uniform theory of diffraction and multiple image theory," *IEEE Transactions on Antennas and Propagation*, 1996.



Reza Aghazadeh (Student Member, IEEE) received his B.Sc. degree in Electronics Engineering from University of Tabriz (Tabriz, Iran) in 2015, and received his M.Sc. degree in Telecommunications Engineering from Politecnico di Milano (Milan, Italy) in 2019, with a thesis on "Analytical outage analysis of mmW systems with cylindrical antenna array". He is pursuing Ph.D. degree at Politecnico di Milano with main focus on signal processing for reconfigurable intelligent surfaces. His main areas of interest include stochastic geometry, aggregated interference analysis and signal processing for wireless communications.



Dario Tagliaferri (Member, IEEE) received the B.Sc. degree (2012), the M.Sc. degree (2015) in Telecommunication Engineering (with honors) and the PhD (2019) in Information Engineering from Politecnico di Milano, Italy. He is currently Assistant Professor at Dipartimento di Elettronica, Informazione e Bioingegneria (DEIB), Politecnico di Milano, Italy, in the framework of Huawei-Polimi Joint Research Lab and the Italian national resilience plan (PNRR PE14 project "RESTART"). His research interests comprise signal processing techniques for wireless communication and sensing systems, with an em-

phasis on vehicular applications. Specific research topics include integrated sensing and communication systems, intelligent reflecting surfaces, V2X communication systems and radar sensing for automotive applications. He was the co-recipient of the Best Paper Awards from the 1st IEEE International Online Symposium on JC&S 2021 and from the EuMA Mediterranean Microwave Symposium 2022. He served as a TPC member in VTC Spring 2022 and currently serving in VTC Spring 2023.



Filippo Morandi (Student Member, IEEE) received the M.Sc. degree in Telecommunication Engineering in 2021 from Politecnico di Milano (Milan, Italy), with a thesis on vehicular communications for mmWave 5G and Beyond applications. He is currently pursuing an industrial Ph.D. within the Huawei-Politecnico di Milano Joint Research Lab, focused on modeling and algorithms for next generation high frequency technologies. His main areas of interest include Free Space Optics (FSO) systems, statistical signal processing, propagation and system modeling. He has also gained expertise by working on activities related to U6G systems, from propagation to large scale coexistence studies, and statistical analysis of antenna arrays emissions in support of standardization activities.



Luca Rinaldi (Student Member, IEEE) received B.Sc. and M.Sc. degrees in Telecommunication Engineering from Politecnico di Milano, Milan, Italy, in 2017 and 2020, respectively. He is a former PhD student at the Dipartimento di Elettronica, Informazione e Bioingegneria, Politecnico di Milano. His main research interests focus on V2X communications and integrated sensing and communication systems for B5G wireless networks.



Laura Resteghini (Member, IEEE) received her M.Sc. degree in Telecommunication Engineering from Politecnico di Milano, Italy in 2009 and the Ph.D. degree in Information Technology from Politecnico di Milano, Italy in 2014. Her experience grew across researches about E.M. wave propagation through the atmosphere at radio frequencies: physical and statistical modeling for E.M. propagation applications also implementing optimization strategies for Fade Mitigation Techniques in Satcom systems. Since 2014 she has been involved in several project related to 5G NR network taking care of the design of prototypes and antenna modelling for mmW bands. In 2016 she joined the Milan R&D center of Huawei Technologies Italia as Senior Microwave Antenna Engineer. She takes care of the synthesis and design of Unconventional Antenna Array for 5G mmW Base Station. She is coordinating the "Sub-THz & Photonic Technologies" working group of the JointLab of Huawei-Polimi.



Christian Mazzucco (Member, IEEE) joined Huawei Technologies, Italy, in 2009, developing high-speed LDPC decoders, algorithms for high-power amplifiers digital predistortion, phase noise suppression, and MIMO for point-to-point microwave links. In 2015 joined the HF 5G Wireless Team that is currently leading and researching on antennas, phased array and MIMO processing and in the development of mmWave 5G NR BTS systems. In the framework of Huawei-Polimi Joint Research Lab he is coordinating different studies on Harmonized Communication and Sensing, V2X, 5G and B5G systems and Sub-THz and Photonics technologies.



Umberto Spagnolini (Senior Member, IEEE) is Professor of Statistical Signal Processing, Director of Joint Lab Huawei-Politecnico di Milano and Huawei Industry Chair at Politecnico di Milano. His research in statistical signal processing covers remote sensing and communication systems with more than 380 papers on peer-reviewed journals/conferences and patents. He is author of the book *Statistical Signal Processing in Engineering* (J. Wiley, 2017). Interests include mmW channel estimation and space-time processing

for single/multi-user wireless communication systems, cooperative and distributed inference methods including V2X systems, mmWave communication systems, parameter estimation/tracking, focusing and wavefield interpolation for remote sensing (UWB radar and oil exploration), and integrated communication and sensing. He was recipient/co-recipient of Best Paper Awards on geophysical signal processing methods (from EAGE), array processing (ICASSP 2006), distributed synchronization for wireless sensor networks (SPAWC 2007, WRECOM 2007), 6G joint communication and sensing (JC&S 2021) and SAR imaging for automotive (MMS 2022). He is technical experts of standard-essential patents and IP. He served as part of IEEE Editorial boards as well as member in technical program committees of several conferences for all the areas of interests.